ELSEVIER

Nanomedicine: Nanotechnology, Biology, and Medicine
45 (2022) 102593

nanomedicine
Nanotechnology, Biology, and Medicine

nanomedjournal.com

Poly(lipoic acid)-based nanoparticles as a new therapeutic tool for delivering active molecules

Chiara Castellani, PhD[a], Claudia Maria Radu, PhD[b], Lucia Morillas-Becerril, PhD[c], Ilaria Barison, Msc[a], Federica Menato, Msc[c], Tomaz Michele Do Nascimento, Msc[c], Marny Fedrigo, MD, PhD[a], Alessia Giarraputo, PhD[a], Grazia Maria Virzì, PhD[d,e], Paolo Simioni, MD[b], Cristina Basso, MD, PhD[a], Emanuele Papini, PhD[f], Regina Tavano, PhD[f], Fabrizio Mancin, PhD[c], Giorgio Vescovo, MD, PhD[g], Annalisa Angelini, MD[a,*]

[a]*Dept. of Cardiac, Thoracic and Vascular Sciences and Public Health, University of Padua, Padua, Italy*
[b]*Thrombotic and Hemorrhagic Diseases Unit, Dept. of Medicine, Padua University Hospital, Padua, Italy*
[c]*Dept. of Chemical Sciences, University of Padua, Padua, Italy*
[d]*Dept. of Nephrology, Dialysis and Transplant, San Bortolo Hospital, Vicenza, Italy*
[e]*IRRIV-International Renal Research Institute Vicenza, San Bortolo Hospital, Vicenza, Italy*
[f]*Dept. of Biomedical Sciences and Centre for Innovative Biotechnological Research-CRIBI, University of Padua, Padua, Italy*
[g]*Dept. of Medicine, Padua University Hospital, Padua, Italy*

Revised 26 May 2022

Abstract

Pluronic-coated polylipoic acid-based nanoparticles (F127@PLA-NPs) have great potential as biodegradable nanovectors for delivering active molecules to different organs in complex diseases. In this study we describe the in vivo biodistribution, safety and ability to deliver molecules of F127@PLA-NPs in healthy rats following intravenous administration. Adult rats were injected with 10 mg/kg of rhodamine B-labeled F127@PLA-NPs, and NPs fluorescence and MFI rate were measured by confocal microscopy in whole collected organs. The NPs accumulation rate was maximal in the heart, compared to the other organs. At the cellular level, myocytes and kidney tubular cells showed the highest NPs uptake. Neither histopathological lesion nor thrombogenicity were observed after NPs injection. Finally, F127@PLA-NPs were tested in vitro as miRNAs delivery nanosystem, and they showed good ability in targeting cardiomyocytes.

These results demonstrated that our F127@PLA-NPs constitute a biological, minimally invasive and safe delivery tool targeting organs and cells, such as heart and kidney.

Keywords: Poly (lipoic acid)-based nanoparticles; Biodistribution; Heart disease; Kidney disease; Confocal microscopy

Background

The treatment of many diseases and syndromes, despite the enormous progress of therapies, remains disappointing.

The reason for that is, in many cases, the complex pathophysiology and the impossibility of reaching multiple and specific targets, very often at the molecular level.

In recent years, nanoparticles have been increasingly employed to reach specific targets and deliver drugs, macromolecules, and even sub-genomic molecules.[1]

Several conditions in the cardiovascular field may take advantage of this innovative approach.[2–6] In particular, its

Abbreviations: F127@PLA-NPs, Pluronic-coated polylipoic acid-based nanoparticles; NPs, nanoparticles; SLN, solid lipid nanoparticles; PLA, polymerized lipoic acid derivates; F127@1,2-NPs, based on 1,8-octanediol derivative 1 and Rhodamine B derivative 2; F127@3 RNA-NPs, nanoparticles with monomer 3 mRNA-FAM conjugated.; HL1, murine cardiomyocytes cell line HL1; MFI, mean fluorescence intensity; MFI/stack profile, mean fluorescence intensity measured across the entire stack profile; DIC, differential interference contrast; TF, tissue factor.

* Corresponding author at: Department of Cardiac, Thoracic and Vascular Sciences and Public Health, University of Padua, Via Gabelli, 61, 35100 Padova, Italy.
E-mail address: annalisa.angelini@unipd.it (A. Angelini).

https://doi.org/10.1016/j.nano.2022.102593

application to emerging gene therapies able to re-modulate the molecular mechanisms responsible for the altered pathophysiological pathways could have a tremendous therapeutic impact.[5,6] Upon the identification of miRNAs able to target the involved genes, a crucial challenge in gene therapy is deliver them into specific cells avoiding biological reactions and metabolization.[7,8]

Nanoparticles can address this issue by hiding nucleic acids in their interior avoiding adverse biological responses and metabolization.[9] In the past years, several types of nanoparticles have been studied for the delivery of genetic material, and solid lipid nanoparticles (SLN) were the most used ones.[10–13]

The ultimate success of this methodology was reached in these days with the production of Covid-19 vaccines.[14]

Of course, nanoparticle activity depends on their pharmacokinetic characteristics, which in turn determine those of the payload: tissue distribution, accumulation, degradation, and clearance.[15]

Most of the nanoparticles accumulate in filtering organs as liver and spleen. Coating with hydrophilic molecules as polyethylene glycol (PEG) or zwitterionic species reduces the activation of reticuloendothelial system (RES) and of complement increasing circulation time. The enhanced permeation and retention (EPR) effect favors accumulation in solid tumors.[16] While conjugation with targeting agent lead the nanoparticle to selectively bind to the desired tissues.[17,18] However, little is still known on the possibility of using the coating features to passively target selected organs.[19]

We have recently reported a novel in vitro biocompatible and biodegradable polymeric nanoparticle: the F127@PLA-NPs.[20] In particular, reduced protein absorption, complement activation, capture from cells of the RES and hemolytic activity were observed.[20] On the other hand, the highly crosslinked poly-lipoic core ensured stability against spontaneous degradation, even upon prolonged storage in water, but relatively fast cleavage in the presence of thiols, as glutathione.[20]

As observed for other disulfide-based nanoparticles and materials, this behavior should warrant the release of the loaded drug/molecule only when the target is reached.[21–23]

In addition, the antioxidant properties of lipoic acid allowed our NPs to demonstrate in vitro a potential protective activity against post-ischemia reperfusion. This feature joined with the great versatility in loading different kinds molecules, gives to this approach a wide potential for application in the medical field.[20]

However, the use of nanoparticles for medical applications requires the fulfillment of several requirements. These include favorable nanoparticle pharmacokinetics, safety, and the ability to carry macromolecules, including gene products.

In this study, we investigated in vitro and in vivo, in Sprague Dawley rats, the tissue distribution, accumulation, persistence, and clearance of our new in house F127@**1**-NPs nanoparticles, their safety in terms of tissue injury, activation of inflammation and coagulation, and their potential to carry and deliver new molecules to the heart and splanchnic organs.

Material and methods

Synthesis and characterization of F127@PLA-NPs nanoparticles

In this paper, we use the convention for core-shell structure to name our particles. Accordingly, the outer shell is indicated first, followed by the @ symbol and the core materials. Hence, our nanoparticles with an F127 shell and a polylipoic acid (PLA) core are named F127@PLA-NPs or F127@**n**-NP, where **n** is the number of the precursor used.

Compounds **1–3** were synthesized by standard procedures and fully characterized.

The hydrodynamic particle size (Dynamic Light Scattering, DLS), Z-potential, Transmission electron microscopy (TEM) and Thermogravimetric analysis (TGA) were performed according to the literature.[20,24] RNA content in the solutions was measured with the ThermoFisher Scientific spectrometer Nanodrop following the company instruction (details in the Supplemental materials).

In vitro cell cultures and F127@1,2-NPs or F127@ 3-NPs (mRNA loaded) identification

The murine atrial cardiomyocyte cell line HL1 was obtained from the laboratory of William C. Claycomb (New Orleans, USA)[25] and following Lin et al.[26] At 70–80 % of confluence, HL1 cells were exposed to 3 h to 1 day with F127@1,2-NPs or to 1.5 h to 1 day with F127@**3**-NPs loaded with FAM-labeled mRNA inside.

Samples were analyzed by a confocal microscope DMI6000CS TCS SP8 (Leica Microsystem, Wetzlar, Germany) using a DFC365FX camera and with a z-interval of 1.5 μm using a 63×/0.60 dry objective magnification (image size 1024 × 1024 pixel). Images were processed using the Leica Application Suite (LAS-AF) 3.1.1. Software (Leica Microsystems, Wetzlar, Germany) (more details in the Supplements).

In vivo animal study

Healthy male Sprague-Dawley rats, weighing 200 g, were injected with 2 mg/rat of rhodamine red labeled F127@1,2-NPs via tail vein and randomly killed at different time points (T0, 1 h, 3 h, 1 day, 3 days, 7 days, and 1 and 2 months) from the injection, and blood and organs were collected from the injection. Experiments were approved by the University of Padua Ethical Committee and from Italian National Health Institute (511/2020-PR and 72/2016 – PR). No animal were excluded in this study.

Immunohistochemistry for different cell types identification

Immunohistochemistry was performed according to standard procedures using the following antibodies: anti-smooth muscle cell actin (SMA, 1:100 Dako Cytomation, Milan, Italy), anti-von Willebrand Factor (1:100 Abcam, Prodotti Gianni, Milan, Italy), CD68 (a marker of macrophages and Kupffer cells) (1:100 Abcam, Prodotti Gianni, Milano, Italy), followed by goat anti-rabbit or goat anti-mouse Alexa Fluor 488 secondary antibodies (Abcam, Milano, Italy). Nuclei were counterstained with TOPRO-3 (Invitrogen, Molecular Probes, Eugene, OR).[27,28]

Confocal laser microscopy and image analysis for the uptake quantification of F127@1,2-NPs in organs and different cell types

Digital Image Analysis was performed using Leica Application Suite (LAS-AF) 3.1.1. software.[27]

We studied two different kinetic parameters:

1) Tissue uptake: this value was expressed as the total mean fluorescence intensity/stack profile (MFI/stack profile), which represents the mean fluorescence intensity (expressed as arbitrary unit) obtained by mean gray-scale values measured across the entire image series for each organ. Values reported as mean ± SD (standard deviation)/stack profile. This parameter identifies the intensity of concentration of fluorophores related to F127@1,2-NPs and is considered as the burden of NPs.[27]
2) Tissue retention and clearance: this parameter expressed the persistence of F127@1,2-NPs in each organ and was calculated as the variation of MFI over time. ΔMFI/Δt is the time derivative function representing the rate of change of fluorescence.

Histology for tissue damage and safety evaluation

To examine tissue damage, sections from each organ were stained with hematoxylin and eosin and observed under a light microscope (Leica, DM4000B,Germany).

Immunohistochemistry was performed to[27]:

1- evaluate tissue inflammation using anti-CD45 (anti lymphocytes, Abcam, Prodotti Gianni, Milan, Italy);
2- evaluate F127@1,2-NPs thrombogenicity using anti-Tissue Factor antibody (TF, 1:100)

Slides were analyzed by light microscopy or by confocal microscope DMI6000CS TCS SP8 (Leica Microsystem, Wetzlar, Germany).

Statistical analysis

All statistical analyses were performed using Graphpad Prism 8. All data were presented as mean ± S.D. Comparison between two groups was done by two-tailed Student's *t*-test for unpaired data and Mann-Whitney test. Comparison between more than two groups was assessed by one-way ANOVA. A 5 % difference was defined as statistically significant.[29,30]

Results

F127@1,2-NPs characteristics

In this paper, we use the convention for core-shell structure to name our particles. Accordingly, the outer shell is indicated first, followed by the @ symbol and the core materials. Hence, our nanoparticles with an F127 shell and a polylipoic acid (PLA) core are named F127@PLA-NPs or F127@**n**-NP, where **n** is the number of the precursor used.

Based on our previous screening of biocompatible and biodegradable poly(lipoic acid) NPs, we selected derivative **1**, featuring a 1,8-octanediol spacer connecting two lipoic acid molecules by ester linkages, and derivative **3**, featuring a tetraethylene glycol spacer, as precursors of the nanoparticles polymeric core. In addition, Rhodamine B-lipoic acid derivative **2** was used to label the nanoparticles to study biodistribution in vivo with rat models. Compounds **1**, **2**, and **3** were prepared in good yields form commercially available precursors by standard synthetic protocols, as described in the Supplemental materials. Compound **1** is soluble in acetone, while compound **3** is soluble in both acetone and ethanol. Dynmic light scattering (DLS) analysis revealed that the batches of F127@**1,2**-NP obtained had an average hydrodynamic diameter of 138–162 nm, with size dispersions in the 30 % range (PDI values between 0.06 and 0.10, see Table S1).

TEM analyses confirmed the average sized and formation of spherical nanoparticles. The Z-potential analysis provided values close to zero (Table S2), ensuring the uncharged nature of these nanoparticles. Characterization data of a representative sample are reported in Fig. 1.

Tissue distribution detection and uptake in organs of F127@1,2-NPs

NPs distribution and density in all organs were estimated by fluorescence confocal microscopy image analyzer algorithms. Immediately after injection, the fluorescence of NPs rapidly spread in all organs (Figs. 2A and 3).

The fluorescent signal increased in the heart up to 3 h, reaching a NPs retention of 30.63 ± 10.78 MFI, about 5 times higher than that of the lung (6.81 ± 2.74 MFI) and kidney (6.57 ± 1.66 MFI), and two-fold higher than that observed in the liver (13.93 ± 1.42 MFI) and in the spleen (17.58 ± 7.75 MFI) at the same time point (Figs. 2A and 3).

The mean accumulation rate in the heart was 3.69 MFI/h in the first 3 h, with a maximum rate of 5.29 MFI/h (Fig. 2B) after 1 h. Thereafter, the mean fluorescence intensity of NPs appeared to decrease rapidly, reaching 7.93 ± 1.15 MFI at seven days after injection with the highest rate of NPs clearance one day after injection (−0.61 MFI/h, Fig. 2A and B).

The NPs accumulation rate in the lung was initially rapid, with a value of 15.87 ± 1.13 MFI at 10 min after NPs injection (Fig. 2A). Immediately afterward, this organ showed a fast clearance with the highest clearance rate among the other analyzed organs equal to −9.26 MFI/h 1 h after NPs injection (Fig. 2B).

In the liver, the NPs fluorescence intensity slowly increased over time, reaching both the maximum mean fluorescence value (26.6 ± 5.13 MFI) and the maximum accumulation rate of 0.23 MFI/h 3 days after injection. A similar trend was observed for the spleen, which showed a continuous fluorescence accumulation with a maximum rate of 3.07MFI/h after 1 h of NPs injection and up to three days, with a significant decline thereafter (Fig. 2A and B).

Lower mean fluorescence intensity values were observed in the kidney associated with a maximum accumulation rate of 0.465 MFI/h 3 h after injection (Fig. 2A and B).

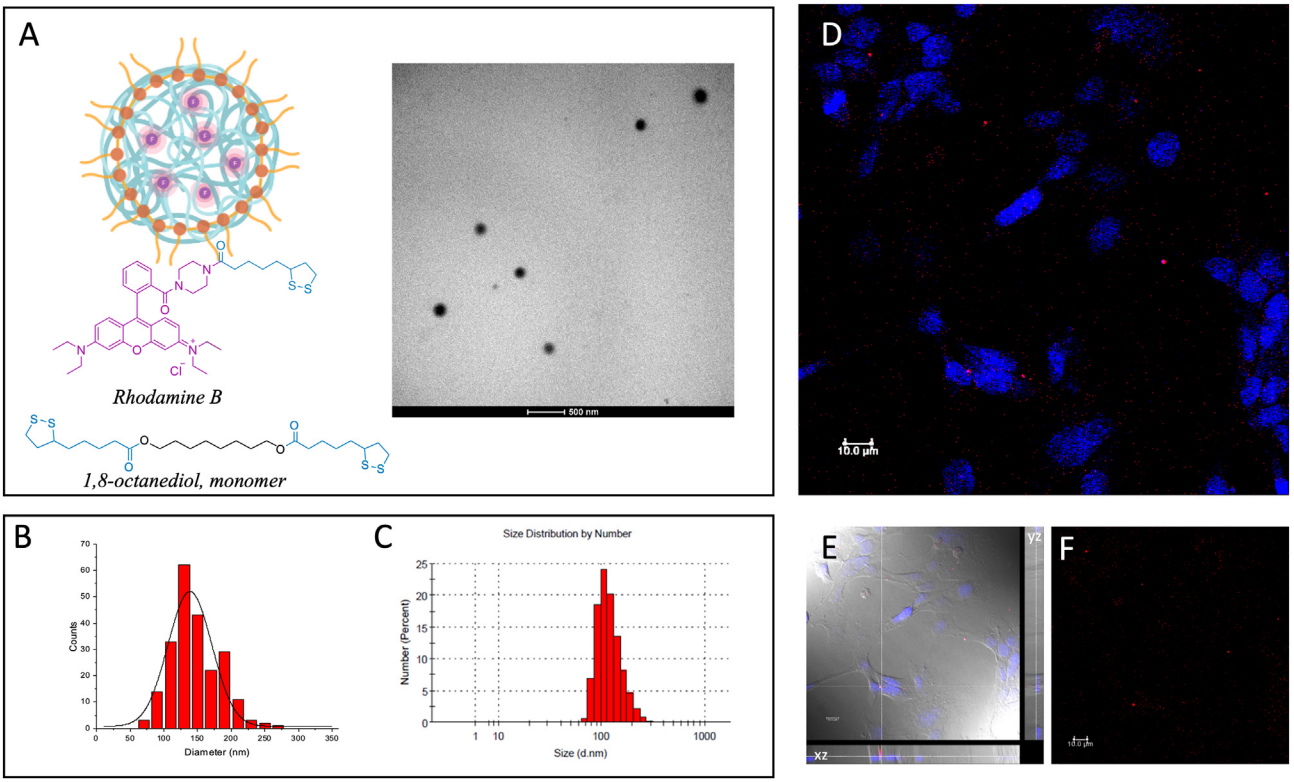

Fig. 1. F127@1,2 NPs rhodamina conjugated. A) on the left: F127@1,2-NP based on 1,8-octanediol derivative 1 and Rhodamine B derivative 2; on the right electron microscopy (TEM) of F127@1,2-NPs. Scale bar indicates 500 nm; B) Nanoparticles size distribution determined by TEM (average size 139 ± 38 nm) of F127@1,2-NPs; C) nanoparticle size distribution (number weighted) determined by DLS of F127@1,2-NPs (average size 138 ± 43 nm, PDI: 0,101); D) representative confocal image of murine atrial cardiomyocytes (HL1) exposed to F127@1,2-NPs for 3 h. Picture highlights NPs in red into the cardiomyocytes. Nuclei were counterstained with TO-PRO3 (in blue). Scale bar indicates 10µm; E) merge of image in D with differential interference contrast (DIC) taken with xyz ortogonal section, which shows morphology of the underling cardiomyocytes. Note as NPs (in red) are located into the myocytes as shown in ortogonal xz section. Scale bar indicates 10 µm. (For interpretation of the references to color in this figure legend, the reader is referred to the web version of this article.)

Quantification of F127@1,2-NPs uptake in different cells types

To understand the capability of different cell types in the studied organs to retain F127@**1,2**-NPs, we used a combination of morphological/immunohistochemistry confocal microscopy.

Image analysis of myocytes showed the highest values of MFI/cell 3 h after injection (25.06 ± 5.126 MFI/cell). At the same time, the fluorescence detected one day and three days after injection inside these cells decreased significantly (16.61 ± 1.266 and 13.06 ± 1.809 MFI/cell respectively, with a $p < 0.0001$ between each time point, Fig. 4A, B and C).

The renal tubular cells showed an opposite trend. NPs accumulation increased during the time, starting with 14.87 ± 2.551 MFI/cell 3 h and after injection and reaching 19.14 ± 3.148 MFI/cell three days after injection (Fig. 4A, D and E). The values of MFI/cell in kidney tubular cells were statistically significant different only between 1d and 3 days after NPs injection (15.82 ± 3.985 and 19.14 ± 3.148 MFI/cell respectively, $p = 0.0007$) (Fig. 4A, D and E).

Hepatocytes showed the lowest MFI/cell value 3 h after injection (13.25 ± 3.354 MFI/cell). The NP fluorescence level increased to a value comparable with tubular cells (18.94 ± 3.033 MFI/cell, $p < 0.0001$) at one day after injection, and continued to grow significantly up to 20.12 ± 3.269 MFI/cell at three days after injection ($p = 0.032$, Fig. 4A, F, and G).

The NP uptake for myocytes, kidney tubular cells and hepatocytes showed an extremely significant difference for all the considered time points and between cell types ($p < 0.0001$, Fig. 4A).

Fig. 2. Tissue distribution and quantification of F127@1,2-NPs uptake in organs.NPs distribution and density in all organs were estimated by fluorescence confocal microscopy image analyzer algorithms. A) Graphs depicted the NPs-fluorescence trend for each organ as MFI/stack profile. Values are reported as mean ± SD; B) graphs show the tissue retention and clearance of NPs in different organs. This parameter expresses the variation of MFI over time. Note as the fluorescent signal increased in the heart up to 3 h, about 5 times higher than that of the lung and kidney and two-fold higher than that observed in the liver and in the spleen at the same time point. The mean accumulation rate in the heart was 3.69 MFI/h in the first 3 h, with a maximum rate of 5.29 MFI/h after 1 h. In the liver, the NPs fluorescence intensity slowly increased over time, reaching both the maximum mean fluorescence value (26.6 ± 5.13 MFI) and the maximum accumulation rate of 0.23 MFI/h 3 days after injection. A similar trend was observed for the spleen.

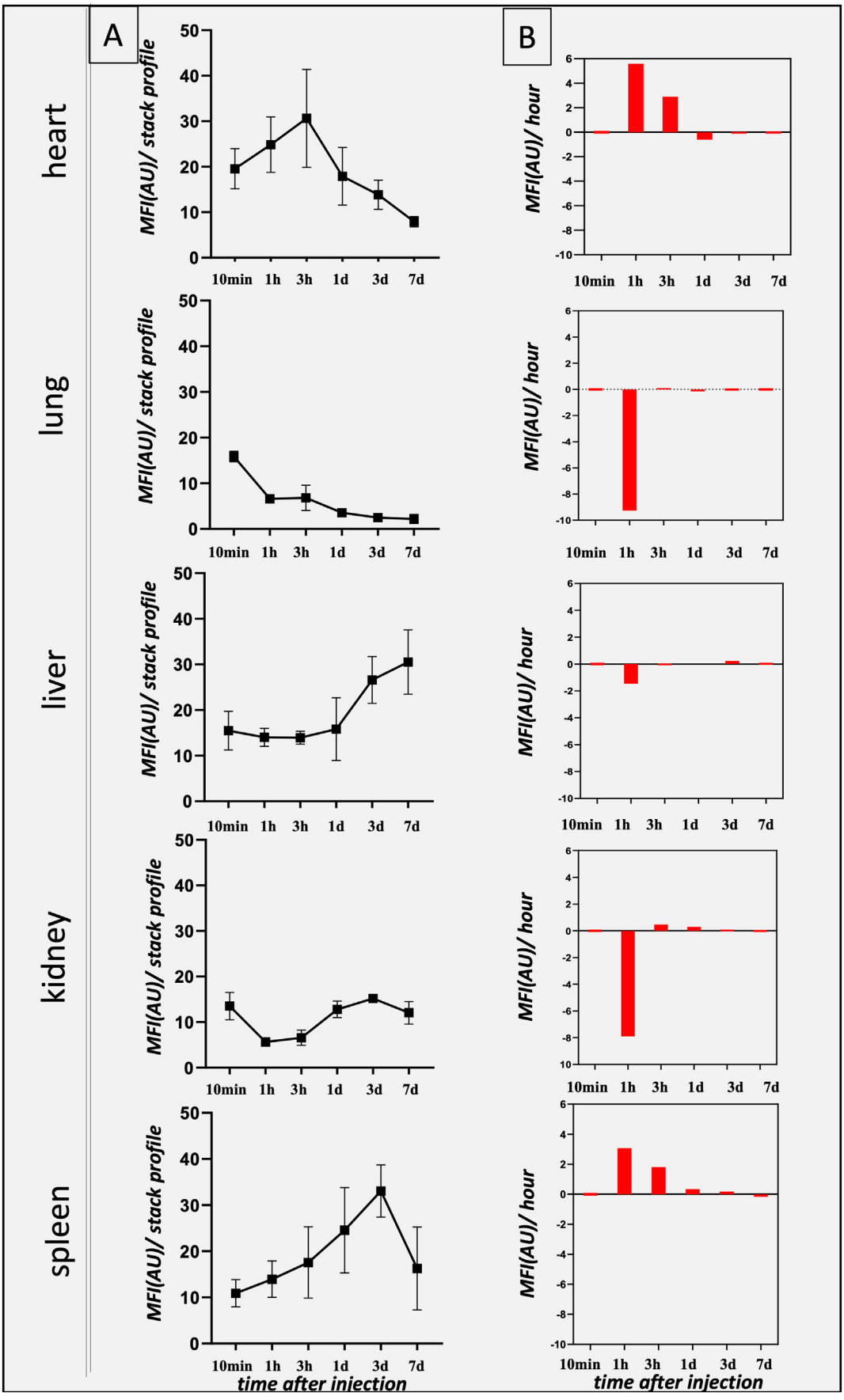
A
B
heart
lung
liver
kidney
spleen
MFI(AU)/ stack profile
MFI(AU)/ hour
10min 1h 3h 1d 3d 7d
time after injection

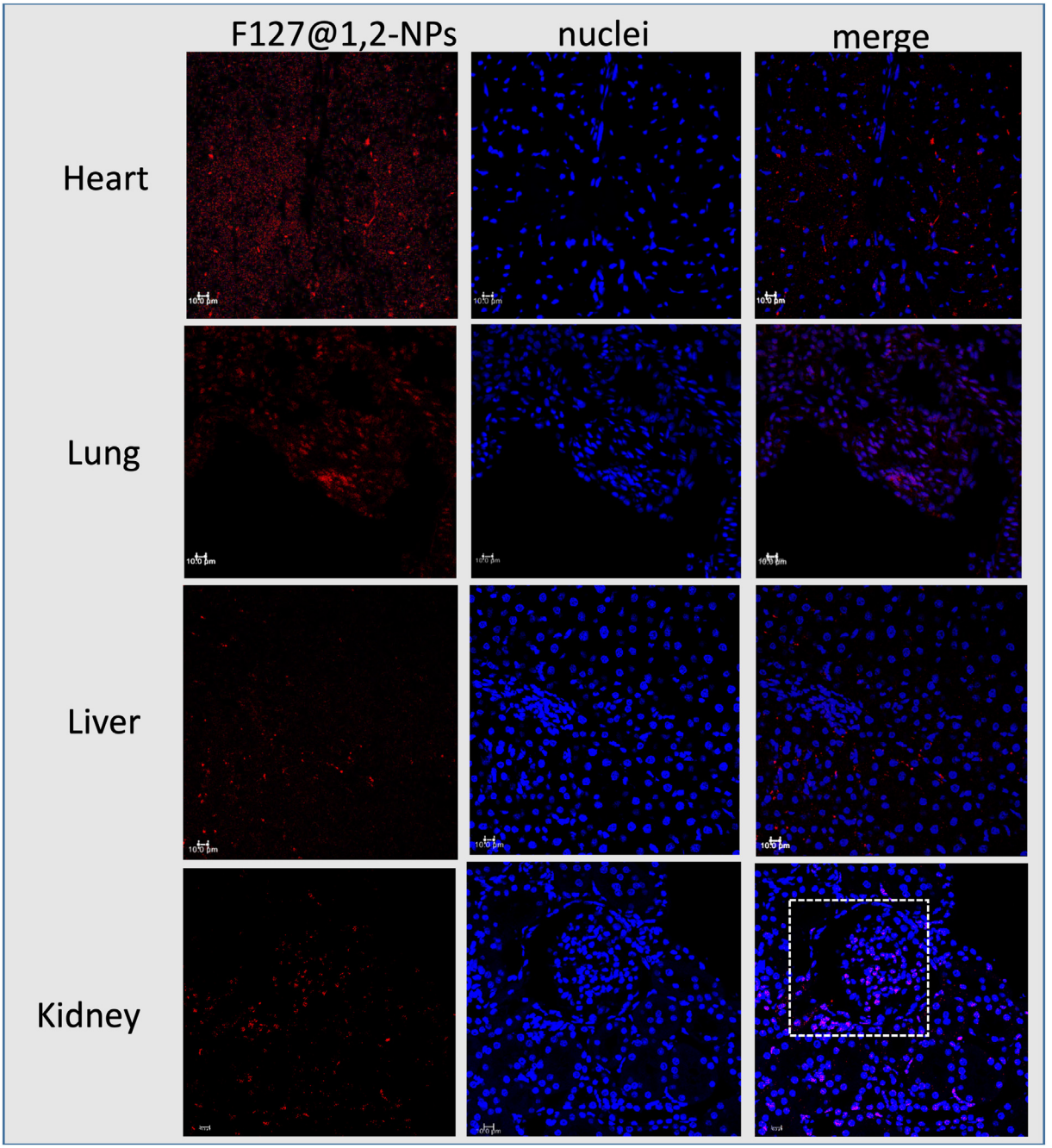

Fig. 3. Microscopic tissue F127@1,2-NPs distribution in different organs at 3 h after injection. NPs (in red) accumulation in different tissues, at 3 h after i.v. injection. Nuclei are counterstained with TO-PRO3 (in blue). Rhodamine-labeled F127@1,2-NPs are more evident in the heart compared to the other organs. In the kidney panel, the white dashed square highlights a glomerulus. Original magnification 40×/0.6. Scale bar indicates 10 μm. (For interpretation of the references to color in this figure legend, the reader is referred to the web version of this article.)

Additionally, we investigated the potential NPs accumulation in other cell types localized in the analyzed organs. We compared the fluorescence level detected in myocytes and vascular cells in the heart, marked with SMA and vWfactor antibodies (Fig. 5). The fluorescence levels between myocytes and vascular cells at 3 h (25.06 ± 5.126 MFI/cell vs. 15.57 ± 1.611 MFI/cell, respectively,) 1d (16.61 ± 1.266 vs 12.49 ± 1.486 MFI/cell respectively) and 3 days (13.06 ± 1.809 vs 9.10 ± 1.135 MFI/cell respectively) showed an extremely statistically significant difference distribution ($p < 0.0001$, Fig. 5B). The analysis revealed that myocytes showed a NPs accumulation almost two-fold higher than vascular cells at 3 h after injection (25.06 ± 5.126 MFI/cell vs. 15.57 ± 1.611 MFI/cell, respectively, $p < 0.0001$) (Fig. 5B). The analysis of fluorescence levels in vascular cells highlighted very statistically significant differences over time. In particular, the analysis of vascular cells distribution reported $p = 0.0047$ between 3 h and 1 day, and $p = 0.0006$ between 1 day and 3 days after injection (Fig. 5B).

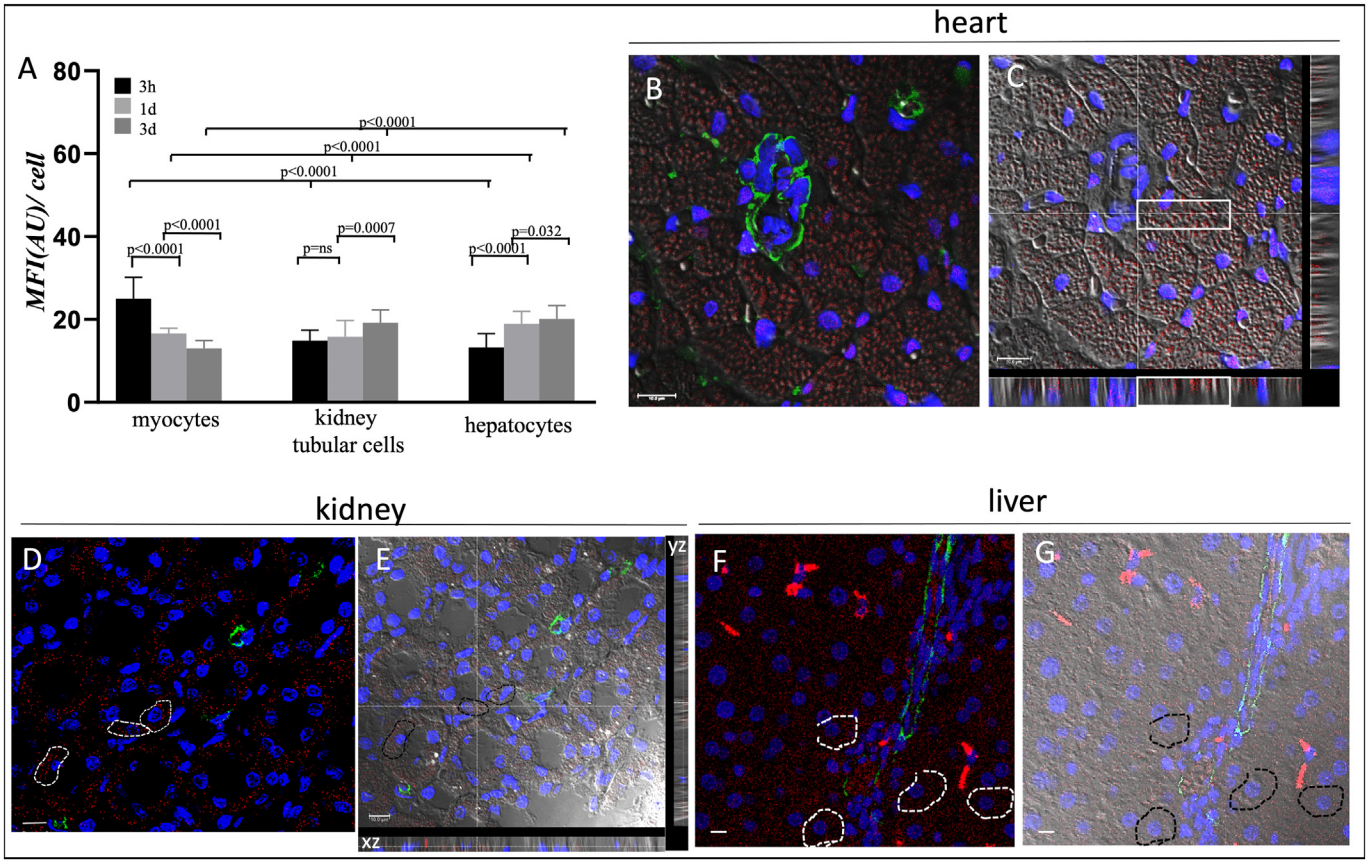

Fig. 4. Quantification of F127@1,2-NPs uptake in different cells types A) graph represents MFI/cell obtained by 3 h, 1 day and 3 days after NPs injection. Data for each cell types are reported as mean ± SD (almost 100 cells/type); B) representative confocal image which highlights the distribution of F127@1,2-NPs (red signal) in myocytes. Nuclei were counterstained with TO-PRO3 (in blue) and SMA for vessels were seen in green. Scale bar indicates 10 μm; C) merge of image in B with differential interference contrast (DIC) taken with xyz orthogonal section, which shows morphology of the underling heart tissue. Note as NPs (in red) are located into the myocytes as shown in white square in orthogonal section. Scale bar indicates 10 μm. Myocytes showed the highest values of MFI/cell 3 h after injection (25.06 ± 5.126 MFI/cell) and decreased significantly ($p < 0.0001$) at three days after injection; D and E) representative confocal laser microscopy images of kidney and merge with DIC (in E) taken with xyz orthogonal section, which show the distribution of NPs in kidney tubular cells (white areas). Scale bar indicates 10 μm; NPs accumulation in kidney tubular cells increased during the time, reaching the maximum value at three days after injection (19.14 ± 3.148 MFI/cell). The values of MFI/cell in kidney tubular cells were significant different only between 1d and 3 days after NPs injection ($p = 0.007$); F and G) representative confocal images highlight the distribution of NPs (in red) in the liver. Nuclei were counterstained with TO-PRO3 (in blue). In G) DIC shows the distribution of NPs into the liver. Scale bar indicates 10 μm. Hepatocytes showed a statistically significant continuous grow up to 3 days after injection ($p = 0.032$). (For interpretation of the references to color in this figure legend, the reader is referred to the web version of this article.)

The kidney behaved very similarly to the heart for fluorescence cells distribution showing that the fluorescence of NPs was 1.6 higher in kidney tubular cells than vascular cells at 3 h after injection (14.87 ± 2.55 vs 8.91 ± 2.63 MFI/cell respectively, $p < 0.0001$; Fig. 6A). At one day after injection, the analysis showed that NPs fluorescence in vascular cells was similar to kidney tubular cells (almost 15.21 ± 4.041 MFI/cell, p = ns; Fig. 6A). At 3 days the difference between tubular cells and vascular cells was due to the increase of kidney tubular cells uptake (19.51 ± 2.910 MFI/cell, $p = 0.009$) (Fig. 6A–E).

Finally, we compared the NPs accumulation between hepatocytes and Kupffer cells, marked with CD68, in the liver, (Fig. 6F). Three hours after injection, NPs were detected mainly in hepatocytes, where the signal was two-fold higher than in Kupffer cells (13.25 ± 3.354 vs.7.366 ± 3.056 MFI/cell respectively, $p < 0.0001$, Fig. 6F). One day after injection, the accumulation trend reversed. The signal associated with NPs present in Kupffer cells was 2-fold higher than that detected in hepatocytes (37.64 ± 19.14 MFI/cell vs 18.94 ± 3.033 MFI/cell respectively, $p = 0.0002$, Fig. 6F). Three days after injection, Kupffer cells still showed a significantly higher accumulation, reaching 48.95 ± 13.10 MFI/cell vs. 20.11 ± 3.387 MFI/cell in hepatocytes ($p < 0.0001$, Fig. 6F, G, H, I).

Histological analysis of tissues after F127@1,2-NPs injection

No mortality was observed in treated animals.

The body weight of the controls and NPs-injected rats exhibited similar increasing trends suggesting that F127@**1,2**-NPs did not interfere with the growth rate of the animals (data not shown).

Histological assessment was performed to examine tissue damage, inflammation and tissue injury from F127@1,2-NPs exposure.

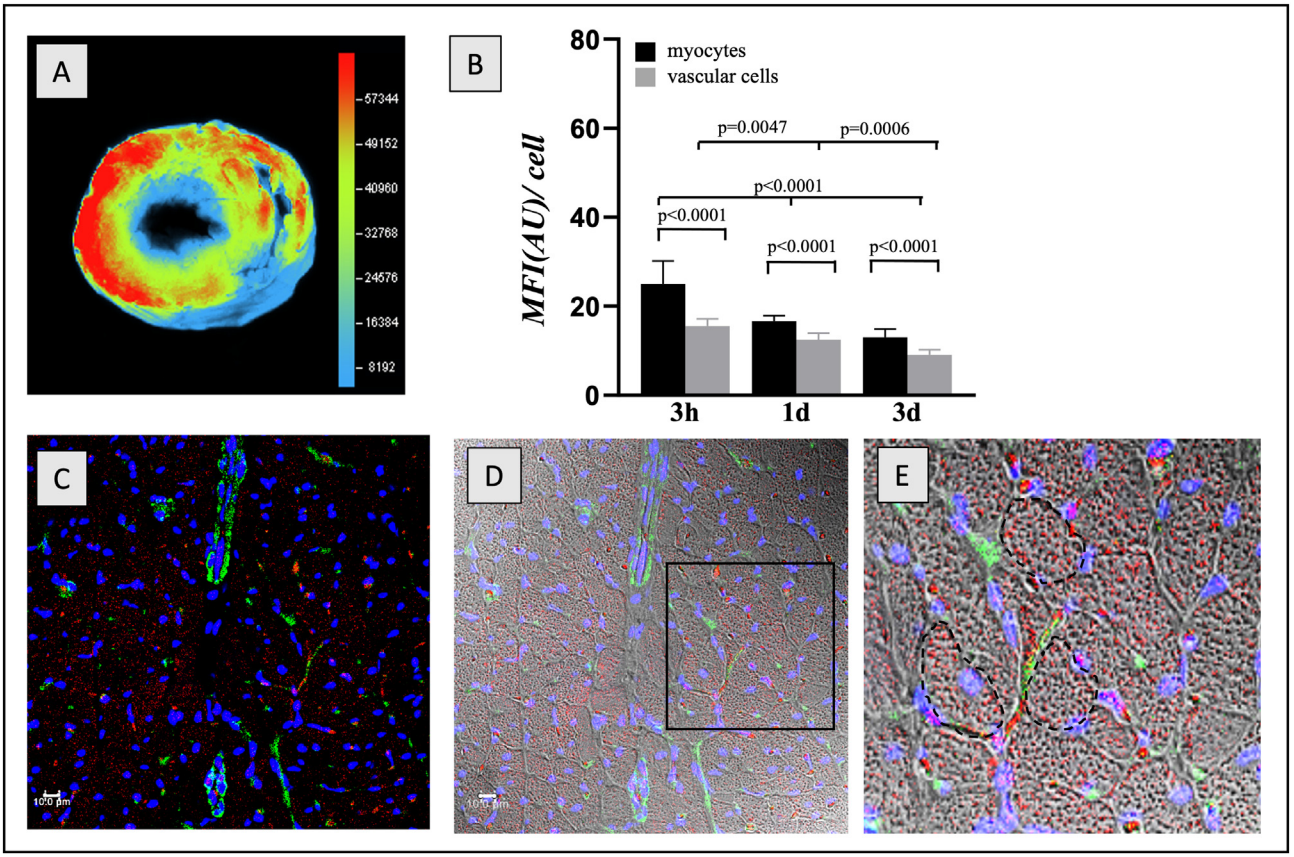

Fig. 5. F127@1,2-NPs localization and uptake in myocytes and vascular cells. A) Macroscopic epifluorescence image of NPs in heart tissue section at 3 h after tail vein injection. The intensity of fluorescence of F127@1,2-NPs (rhodamine coniugated) is represented and normalized as pseudo-color scale bar; B) graph represents the cells mean fluorescence intensity quantification expressed as MFI/cell. Data are reported as mean ± SD (mean of almost 100 cells/field). The fluorescence levels between myocytes and vascular cells showed a statistically significant difference over time (almost $p < 0.0001$), with myocytes reaching the highest value at 3 h after injection; C) representative confocal laser microscopy image of heart section that shows NPs distribution 3 h after injection. F127@1,2-NPs (red signal). SMA positive cells in green highlights vessels in heart section. Nuclei were counterstained with TO-PRO3 (in blue). Scale bar indicates 10 μm; D) merge of image in C with DIC which shows morphology of the underling heart tissue; Scale bar indicates 10 μm; E) zoom image of the black square in D), which demonstrate as NPs (in red) are present in the heart interstitium and in the vessels and in the cytoplasm of the cardiomyocytes (black dashed lines). Zoom from 40×/0.6. (For interpretation of the references to color in this figure legend, the reader is referred to the web version of this article.)

Representative hematoxylin and eosin (H&E) staining results are shown in Fig. 7. Heart, lung, liver, kidney and spleen showed normal morphology and no pathological changes both immediately and one week after NPs injection. In addition, although the liver accumulates a significant proportion of NPs after three days due to the accumulation of NPs in Kupffer cells, no morphological changes were observed even at two months after NPs injection (Fig. 7).

Moreover, in situ detection of Tissue Factor (TF) in the liver vascular endothelial cells showed no signs of over-expression of this marker (Fig. S11).

Finally, heart, kidney, and liver did not show inflammatory cell infiltration at any time after NPs injection (Fig. S12).

Poly(lipoic acid)-based nanoparticles and mRNA encapsulation

To understand if these new NPs can carry and deliver molecules to different organs and cells, we studied F127@**3**-NPs loaded with an mRNA-FAM tag.

F127@**3**,**RNA**-NP had an average hydrodynamic diameter of 100.0 nm with size dispersions in the 64 % range (0.41 PDI value). Efficiency of RNA encapsulation was 63 % (Fig. S9).

Fig. 6. F127@1,2-NPs quantification in kidney and liver. A) graph represents the MFI/cell obtained over time after NPs injection. Data of vascular cells and kidney tubular cells are reported as mean ± SD (mean of almost 100 cells/field). Note that in particular, at 3 days the difference between tubular cells and vascular cells was due to the increase of kidney tubular cells uptake ($p = 0.009$); B) 3D view of representative confocal image depicting the presence of NPs also into vascular cells. Original magnification 40×; C, D and E) 2D zoom of the image in B showing NPs both in vascular and in kidney tubular cells (white ROI). NPs are red, nuclei were counterstained with TO-PRO3 (in blue) and vascular cells are in green. Zoom from original magnification of 63×; F) graph MFI/cell obtained over time after NPs injection. Data are reported as mean ± SD; G) 3D view of representative confocal image that depict the presence of NPs into Kupffer cells in the liver. Original magnification 40 X; H, I and F) 2D zoom of the image in G which underline that NPs (in red) are more associated to Kupffer cells than hepatocytes (white ROI). NPs are in red, nuclei in blue and Kupffer cells (CD68 antibody) are shown in green (I). Zoom from original magnification of 63×. At 1d after NPs injection, the NPs fluorescence was more associate with Kupffer cells than with hepatocytes ($p < 0.0002$). (For interpretation of the references to color in this figure legend, the reader is referred to the web version of this article.)

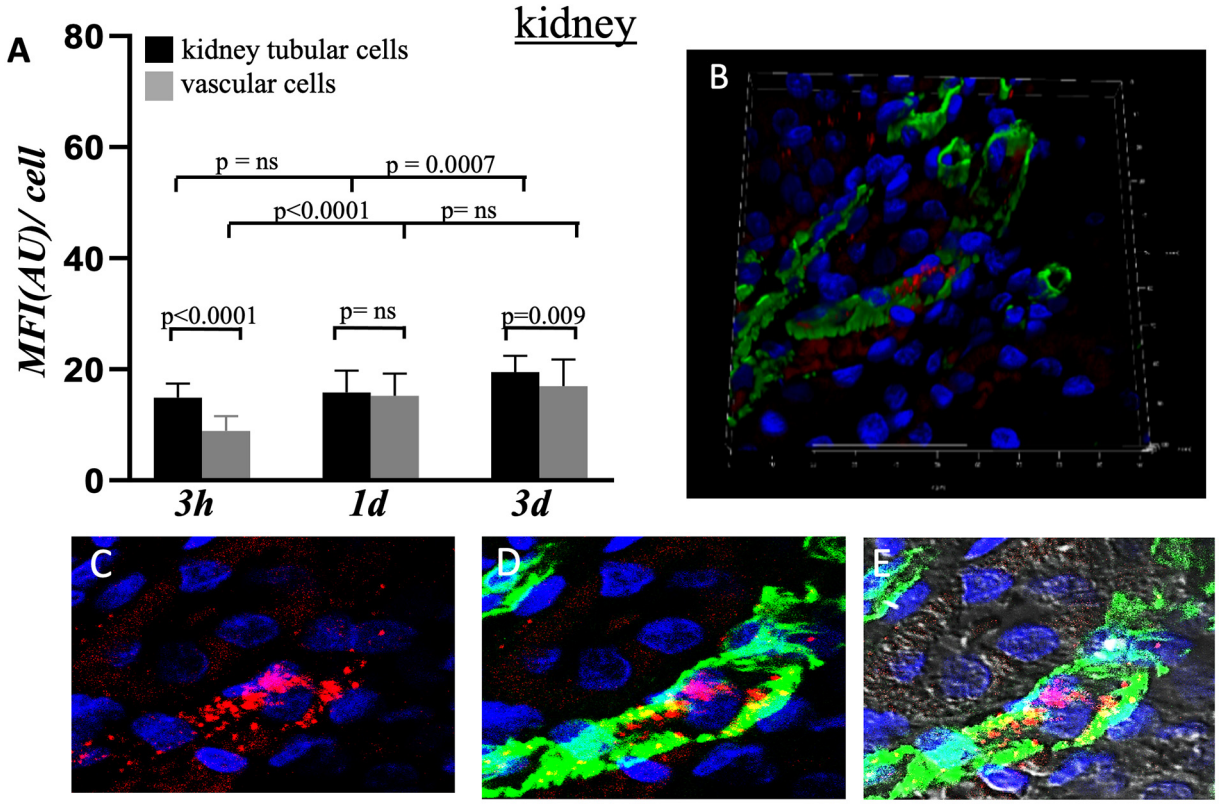
kidney
A
kidney tubular cells
vascular cells
MFI(AU)/ cell
80
60
40
20
0
p = ns
p = 0.0007
p<0.0001
p= ns
p<0.0001
p= ns
p=0.009
3h
1d
3d
B
C
D
E

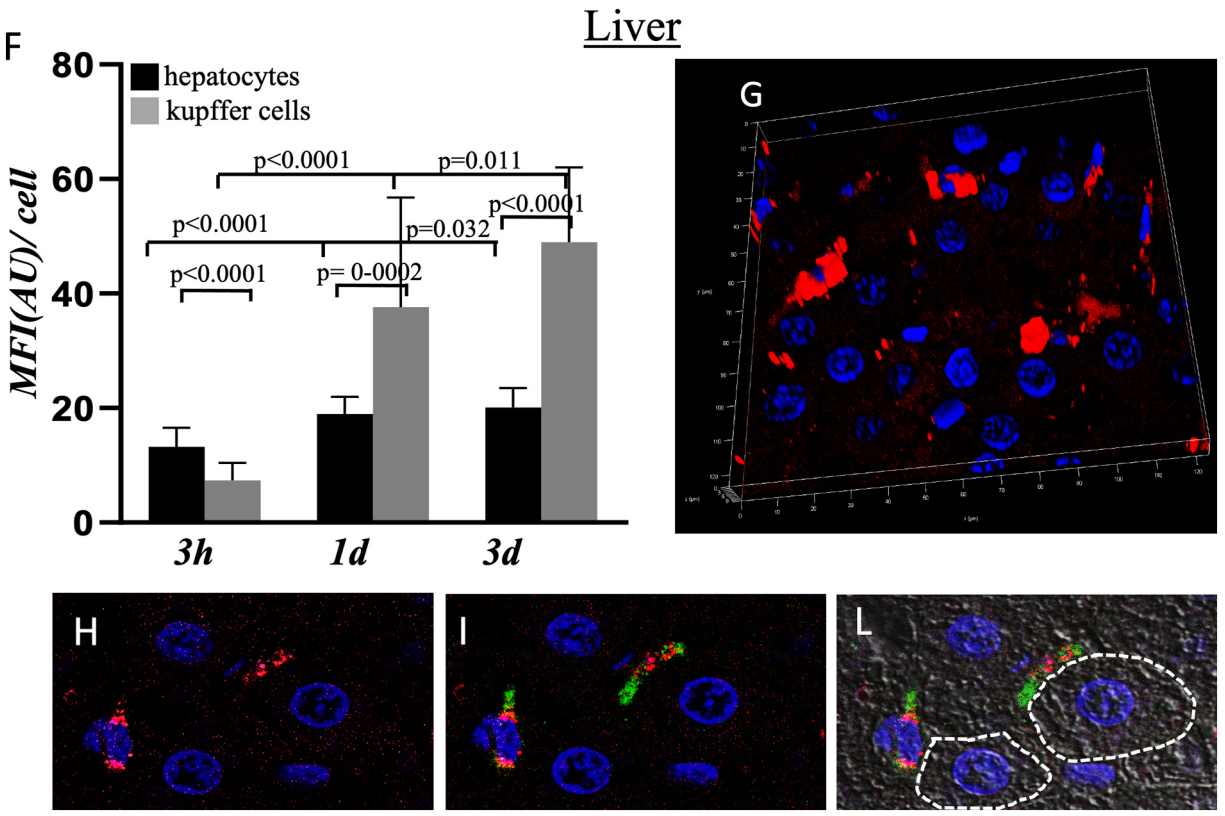
Liver
F
hepatocytes
kupffer cells
MFI(AU)/ cell
80
60
40
20
0
p<0.0001
p=0.011
p<0.0001
p<0.0001
p=0.032
p<0.0001
p= 0-0002
3h
1d
3d
G
H
I
L

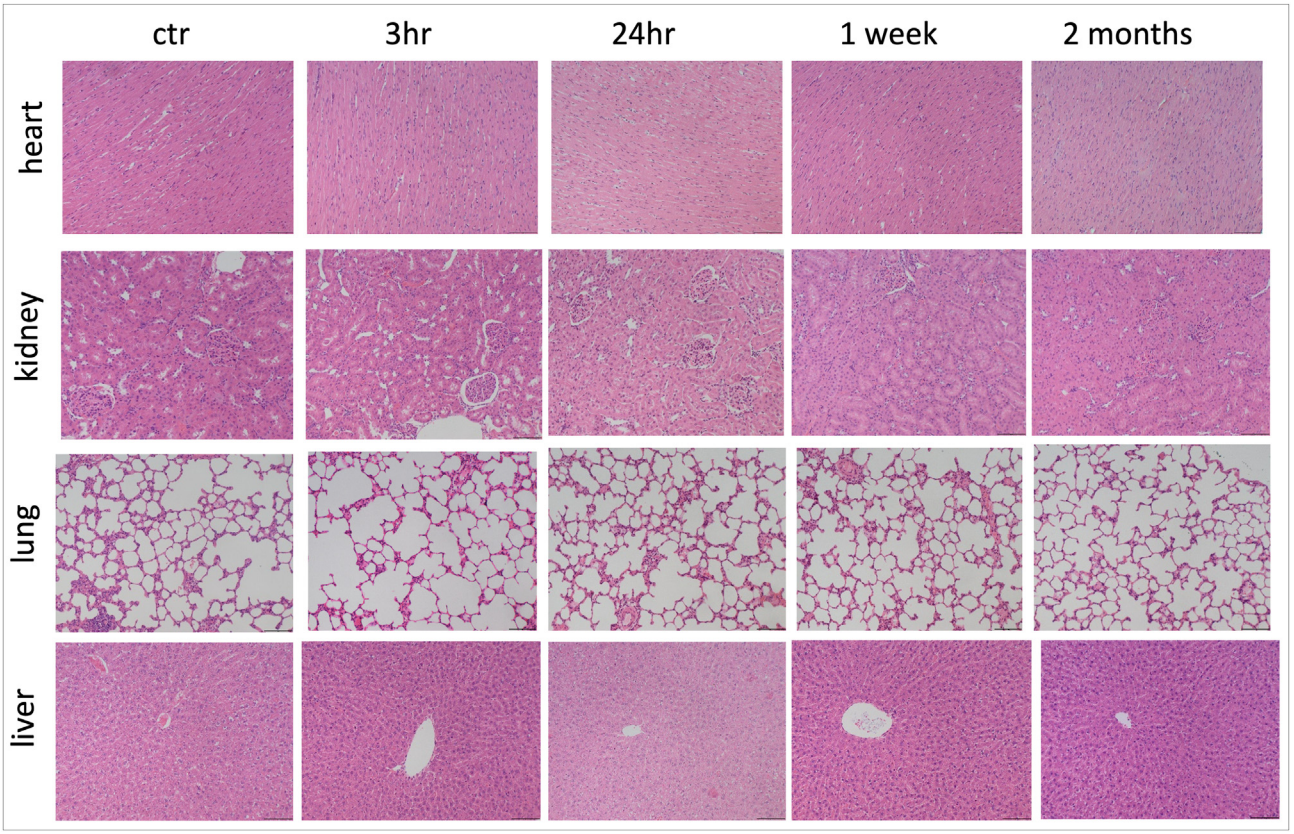

Fig. 7. Hematoxylin and Eosin (H&E) of major organs.H&E staining of heart, lung, kidney, liver and spleen showed normal morphology and no pathological changes both immediately and one week after NPs injection. In addition, although the liver accumulates a significant proportion of NPs after three days due to the accumulation of NPs in Kupffer cells, no morphological changes were observed even at two months after NPs injection. In particular, no signs of necrosis are present. Original magnification 10×.

Treatment of murine atrial cardiomyocytes cell line HL1 with these NPs confirms their ability to enter the cells and likely release their "cargo" into the cells (Fig. 8A–C). In addition, the 3D confocal analysis showed mRNA (in yellow) inside the cells and localized near the cardiomyocytes nuclei (Fig. 8B–E).

Discussion

In this paper, we have demonstrated that F127@PLA-NPs injected intravenously can be successfully delivered to various organs.

Interestingly, the behavior observed is different from the typical ones of PEGylated nanoparticles. In most of the cases, these accumulate first in filtering organs, as liver and spleen, with significantly higher concentrations than in other organs.[3,31–35] Initial accumulation in highly vascularized organs, as lungs, is also observed in a smaller number of cases. Accumulation in kidneys occurs later, as well as, in a limited number of reported cases, in the heart.[36–41]

By the contrary our NPs were rapidly and selectively incorporated in the heart, with a subsequent slow redistribution in liver, spleen and kidneys.

Preferential accumulation in the hearts was reported previously only for PEGylated solid lipid nanoparticles (SLN), but their kinetic uptake was not investigated.[42–44] Noteworthy, structure and general properties of PEGylated SLN and our NP should be quite similar. In both of the cases, they feature a neutral hydrophilic outer shell that encloses a lipophilic core made respectively by cholesterol and polymerized lipoic acid derivatives. This structure is likely responsible for the unusually low adsorption of plasma proteins previously observed, and likely also for the fast heart accumulation.

We observed that concentration of NPs in the heart reaches their maximum in 3 h but declines relatively slowly with 30 % of the total still present at seven days. The subsequent increasing trend in NPs accumulation over time in liver and spleen, which reaches a maximum at days 3–7, is probably due to a gradual redistribution of NPs from other tissue as previously underlined by Daems e coworkers.[45]

In the kidney, the maximal accumulation also was observed after three days and persisted unchanged at day seven, in keeping with the slow degradation of the nanoparticles, which were too large to pass the renal filters. It is important to underline that the whole kinetic behavior and organ retention of our NPs fully supports the effective inclusion of dye 2 in the polymerized core before tissue uptake, since in the case of early degradation occurrence renal clearance would be expected.

The data so far discussed are very important for identifying therapeutic windows, when drugs or molecules acting on both organs have to be used. In addition, since organ distribution does

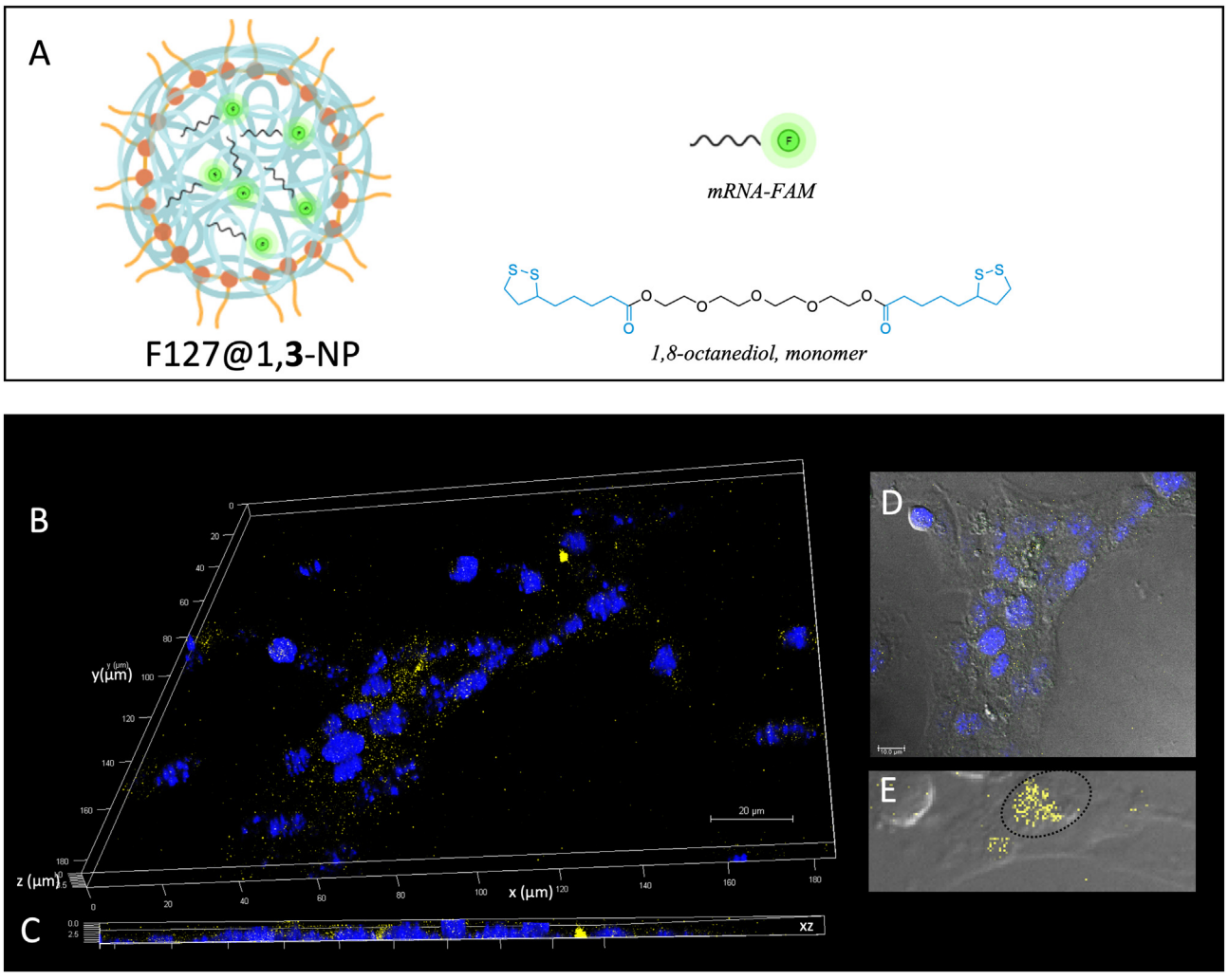

Fig. 8. Evidence of NPs loaded with mRNA-FAM conjugated in vitro.A) Schematic representation of F127@3-NP based on 1,8-octanediol, monomer 1, and mRNA-FAM conjugated; B) confocal microscopy 3D projection showing murine atrial cardiomyocytes cell line HL1 at 1 h after treatment with NPs loaded with mRNA-FAM conjugated. Note as the mRNA (FAM in yellow) is present into the cardiomyocytes and near the nuclei counter-stained with TO-PRO3 (in blue). Scale bar indicates 20 µm. Treatment of murine atrial cardiomyocytes with these NPs confirms their ability to enter the cells and likely release their "cargo" into the cells; C) orthogonal yz section highlights mRNA molecules into the cardiomyocytes. D) representative 2D confocal image of cardiomyocytes with differential interference contrast (DIC, in gray) which shows morphology of the underling cells. Nuclei were counterstained with TO-PRO3 (in blue) and mRNA conjugated with FAM (in yellow). Scale bar indicates 10 µm; E) zoom of representative confocal image that shows mRNA (in yellow). Zoom from 63×. (For interpretation of the references to color in this figure legend, the reader is referred to the web version of this article.)

not necessarily reflect the accumulation in the different cell populations that form the entire organ, we looked at single cells types, especially those that could constitute the target of therapeutic interventions in cardiovascular syndromes.

We have found that NPs, beside in interstitial and endothelial cells, were present and retained in cardiomyocytes, kidney tubular cells and hepatocytes. In particular, the distribution of NPs in cardiac vascular cells and cardiomyocytes was almost identical at three days. Zhang and coworkers[46] also reported that cardiac cells were able to internalize nanoparticles by endocytosis mediated by lipid raft and actin more than by clathrin in FITC-PEG-SPIONs NPs uptake.

Actually, the mechanism underlying the accumulation of our in-house F127@PLA-NPs in the cardiomyocytes is not known and studies aim to clarify the key pathway of the cardiac cells' uptake are ongoing.

Our results may be of particular relevance for the applicability NP as drug nanovectors in one of the most complex syndromes in the cardiovascular field, namely, the cardiorenal syndromes.

Cardiorenal syndromes are characterized by an intricate cross-talk between the failing heart and the kidneys with alterations in hemodynamic, neurohormonal, and inflammatory responses that lead to molecular derangement very often specific for different phenotypes.[47,48]

We have recently found that in CRS type II, NGAL/MMP9 complexes play a significant role in perpetuating the vicious cycle of heart and kidney morphologic adverse remodeling.[28,49] So far, no pharmacological interventions have led to the

interruption of this cycle, but genomic therapy delivering miRNA utilizing NPs may open a new therapeutic avenue.

This has been already applied in myocardial infarction and ischemic-reperfusion injury animal models in which miRNA loaded in different types of nanoparticles were used to block cardiomyocytes apoptosis, myocardial inflammation and to promote cardiomyocytes proliferation.[50–55]

Another critical issue of the present paper is the safety profile of NPs. We have shown with normal histology that no tissue damage is present, especially in terms of inflammation or tissue necrosis. Furthermore, thrombogenicity, which is one of the most feared side effects with therapies employing NPs, has not been observed in that no tissue factor activation has been found in any of the studied organs. Tissue factor (TF), the 47 kDa membrane-bound glycoprotein, is always present on sub-endothelial cells under normal physiological conditions. Endothelial damage exposes TF to the bloodstream activating the coagulation protease cascades and promoting thrombotic episodes.[56] We have shown that NPs injection did not induce endothelial injury and the consequent activation of sub-endothelial TF expression, indicating that our F127@PLA-NPs did not promote thrombi formation.

These data are in keeping with our previous work[20] in which we have already demonstrated the in vitro cell compatibility of these NPs using blood leukocytes and red blood cells. As well, we showed lack of procoagulant activity in vitro in human plasma. Moreover, NPs were already shown to have poor protein adsorbing properties in human serum, plasma and other complex protein matrix.

The data on NPs pharmacokinetic are undoubtedly essential, but it can be argued that for granting a therapeutic effect, it has to be demonstrated that drugs, molecules, or miRNAs have to be delivered into cells once carried by the NPs.

This question has been partially answered in this paper since we have shown that mRNAs are carried and delivered into the cultured myocytes by NPs in vitro. Furthermore, mRNAs are localized predominantly in the perinuclear area, similar to that found for NPs in the in vivo experiments. Ruiz-Esparza et al.[57] also reported that cardiac cells are able to internalize and traffic nanoparticles to the perinuclear cellular regions. These preliminary data represent a proof of concept that miRNA can be loaded on our F127@PLA-NPs and delivered to intracellular space. In the future, the therapeutic effect and the ability of the NPs to deliver mRNA to specific organs needs to be demonstrated in vivo animal models of disease and later on patients.

In conclusion, we think that this paper answers the main questions we previously posed on NPs, in particular kinetic, organs distribution and retention, safety, and ability to carry and deliver miRNAs at the intracellular level.

Sources of funding

This work was supported by the University of Padua grants: CPDA149379, BIRD199570, BIRD204045 and by UE MSCA-ITN grants MMBio (contract n. 721613) and DIRNANO (contract n. 956544).

Disclosures

None.

CRediT authorship contribution statement

Castellani C.: Conceptualization, Funding acquisition, Data duration, Formal analysis, Investigation, Methodology, Supervision, Validation, Writing original draft, Writing - review & editing.

Radu C.M.: Formal analysis, Methodology, Writing - review & editing.

Morillas-Becerril L.: Investigation, Methodology, Writing.

Barison I.: Investigation, Methodology, Original draft, Writing - review & editing.

Menato F.: Investigation, Methodology.

Do Nascimento T.M.: Investigation, Methodology.

Fedrigo M.: Data curation, Review & editing.

Giarraputo A.: Data curation, Methodology, Review & editing.

Virzì G.M.: Data curation, Review & editing.

Simioni P.: Review & editing.

Basso C.: Review & editing.

Papini E.: Data curation, Review & editing.

Tavano R.: Data curation, Review & editing.

Mancin F.: Conceptualization, Funding acquisition, Project administration, Supervision, Writing original draft, Validation, Writing - review & editing.

Vescovo G.: Conceptualization, Funding acquisition, Project administration, Supervision, Validation, Writing original draft, Writing - review & editing.

Angelini A.: Conceptualization, Funding acquisition, Project administration, Supervision, Validation, Writing original draft, Writing - review & editing.

Appendix A. Supplementary data

Supplementary data to this article can be found online at https://doi.org/10.1016/j.nano.2022.102593.

References

1. del Pozo-Rodríguez A, Delgado D, Solinís MÁ, et al. Solid lipid nanoparticles as potential tools for gene therapy: in vivo protein expression after intravenous administration. *Int J Pharm* 2010;**385**(1–2):157-62, https://doi.org/10.1016/j.ijpharm.2009.10.020.
2. Bheri S, Davis ME. Nanoparticle-hydrogel system for post-myocardial infarction delivery of MicroRNA. *ACS Nano* 2019;**13**(9):9702-6, https://doi.org/10.1021/acsnano.9b05716.
3. Wang Q, Song Y, Chen J, et al. Direct in vivo reprogramming with non-viral sequential targeting nanoparticles promotes cardiac regeneration. *Biomaterials* 2021;**276**(February)121028, https://doi.org/10.1016/j.biomaterials.2021.121028.
4. Fan C, Joshi J, Li F, et al. Nanoparticle-mediated drug delivery for treatment of ischemic heart disease. *Front Bioeng Biotechnol* 2020;**8**(June):1-13, https://doi.org/10.3389/fbioe.2020.00687.
5. Richart AL, Reddy M, Khalaji M, et al. Apo AI nanoparticles delivered post myocardial infarction moderate inflammation. *Circ Res* 2020: 1422-36, https://doi.org/10.1161/CIRCRESAHA.120.316848 Published online.

6. Boada C, Zinger A, Tsao C, et al. Rapamycin-loaded biomimetic nanoparticles reverse vascular inflammation. *Circ Res* 2020:25-37, https://doi.org/10.1161/CIRCRESAHA.119.315185 Published online.
7. Thomson DW, Bracken CP, Goodall GJ. Experimental strategies for microRNA target identification. *Nucleic Acids Res* 2011;**39**(16):6845-53, https://doi.org/10.1093/nar/gkr330.
8. Jin G, Li W, Song F, et al. Fluorescent conjugated polymer nanovector for in vivo tracking and regulating the fate of stem cells for restoring infarcted myocardium. *Acta Biomater* 2020;**109**:195-207, https://doi.org/10.1016/j.actbio.2020.04.010.
9. Cassani M, Fernandes S, Vrbsky J, Ergir E, Cavalieri F, Forte G. Combining nanomaterials and developmental pathways to design new treatments for cardiac regeneration: the pulsing heart of advanced therapies. *Front Bioeng Biotechnol* 2020;**8**(April), https://doi.org/10.3389/fbioe.2020.00323.
10. Guo J, Wan T, Li B, et al. Rational Design of Poly(disulfide)s as a universal platform for delivery of CRISPR-Cas9 machineries toward therapeutic genome editing. *ACS Cent Sci* 2021;**7**(6):990-1000, https://doi.org/10.1021/acscentsci.0c01648.
11. Sikora KN, Castellanos-García LJ, Hardie JM, et al. Nanodelivery vehicles induce remote biochemical changes: in vivo. *Nanoscale* 2021;**13**(29):12623-33, https://doi.org/10.1039/d1nr02563e.
12. Lobovkina T, Jacobson GB, Gonzalez-Gonzalez E, et al. In vivo sustained release of siRNA from solid lipid nanoparticles. *ACS Nano* 2011;**5**(12):9977-83, https://doi.org/10.1021/nn203745n.
13. Maurer N, Wong KF, Stark H, et al. Spontaneous entrapment of polynucleotides upon electrostatic interaction with ethanol-destabilized cationic liposomes. *Biophys J* 2001;**80**(5):2310-26, https://doi.org/10.1016/S0006-3495(01)76202-9.
14. Hou X, Zaks T, Langer R, Dong Y. Lipid nanoparticles for mRNA delivery. *Nat Rev Mater* 2021, https://doi.org/10.1038/s41578-021-00358-0 0123456789.
15. Tyler P, Kang P. Diagnostic and therapeutic nanoparticles in cardiovascular diseases. *Curr Pharm Des* 2015;**21**(42):6070-80, https://doi.org/10.2174/1381612821666151027151957.
16. Huynh E, Zheng G. Cancer nanomedicine: addressing the dark side of the enhanced permeability and retention effect. *Nanomedicine (Lond)* 2015;**10**(13):1993-5, https://doi.org/10.2217/nnm.15.86.
17. Alam N, Koul M, Mintoo MJ, et al. Development and characterization of hyaluronic acid modified PLGA based nanoparticles for improved efficacy of cisplatin in solid tumor. *Biomed Pharmacother* 2017;**95**(May):856-64, https://doi.org/10.1016/j.biopha.2017.08.108.
18. Morillas-Becerril L, Peta E, Gabrielli L, et al. Multifunctional, CD44v6-targeted ORMOSIL nanoparticles enhance drugs toxicity in cancer cells. *Nanomaterials* 2020;**10**(2):1-21, https://doi.org/10.3390/nano10020298.
19. Attia MF, Anton N, Wallyn J, Omran Z, Vandamme TF. An overview of active and passive targeting strategies to improve the nanocarriers efficiency to tumour sites. *J Pharm Pharmacol* 2019;**71**(8):1185-98, https://doi.org/10.1111/jphp.13098.
20. Trzciński JW, Morillas-Becerril L, Scarpa S, et al. Poly(lipoic acid)-based nanoparticles as self-organized, biocompatible, and Corona-free nanovectors. *Biomacromolecules* 2021;**22**(2):467-80, https://doi.org/10.1021/acs.biomac.0c01321.
21. Maggini L, Cabrera I, Ruiz-Carretero A, Prasetyanto EA, Robinet E, De Cola L. Breakable mesoporous silica nanoparticles for targeted drug delivery. *Nanoscale* 2016;**8**(13):7240-7, https://doi.org/10.1039/c5nr09112h.
22. Picchetti P, Moreno-Alcántar G, Talamini L, Mourgout A, Aliprandi A, De Cola L. Smart nanocages as a tool for controlling supramolecular aggregation. *J Am Chem Soc* 2021;**143**(20):7681-7, https://doi.org/10.1021/jacs.1c00444.
23. Talamini L, Picchetti P, Ferreira LM, et al. Organosilica cages target hepatic sinusoidal endothelial cells avoiding macrophage filtering. *ACS Nano* 2021;**15**(6):9701-16, https://doi.org/10.1021/acsnano.1c00316.
24. Bellini C, Antonucci S, Morillas-becerril L, Scarpa S, Tavano R. Nanoparticles based on cross-linked poly (lipoic acid) protect macrophages and cardiomyocytes from oxidative stress and ischemia reperfusion injury. *Antioxidants* 2022;**11**(5):907, https://doi.org/10.3390/antiox11050907.
25. Claycomb WC, Lanson NA, Stallworth BS, et al. HL-1 cells: a cardiac muscle cell line that contracts and retains phenotypic characteristics of the adult cardiomyocyte. *Proc Natl Acad Sci U S A* 1998;**95**(6):2979-84, https://doi.org/10.1073/pnas.95.6.2979.
26. Lin CD, Radu CM, Vitiello G, et al. Sounds stimulation on in vitro hl1 cells: a pilot study and a theoretical physical model. *Int J Mol Sci* 2021;**22**(1):1-22, https://doi.org/10.3390/ijms22010156.
27. Castellani C, Fedrigo M, Tavano R, et al. Tumor-facing hepatocytes significantly contribute to mild hyperthermia-induced targeting of rat liver metastasis by PLGA-NPs. *Int J Pharm* 2019;**566**(May):541-8, https://doi.org/10.1016/j.ijpharm.2019.06.004.
28. Vescovo G, Castellani C, Fedrigo M, et al. Stem cells transplantation positively modulates the heart-kidney cross talk in cardiorenal syndrome type II. *Int J Cardiol* 2019;**275**:136-44, https://doi.org/10.1016/j.ijcard.2018.10.038.
29. Angelini A, Castellani C, Ravara B, et al. Stem-cell therapy in an experimental model of pulmonary hypertension and right heart failure: role of paracrine and neurohormonal milieu in the remodeling process. *J Hear Lung Transplant* 2011;**30**(11):1281-93, https://doi.org/10.1016/j.healun.2011.07.017.
30. Castellani C, Vescovo G, Ravara B, et al. The contribution of stem cell therapy to skeletal muscle remodeling in heart failure. *Int J Cardiol* 2013;**168**(3):2014-21, https://doi.org/10.1016/j.ijcard.2013.01.168.
31. Arnida Janát-Amsbury MM, Ray A, Peterson CM, Ghandehari H. Geometry and surface characteristics of gold nanoparticles influence their biodistribution and uptake by macrophages. *Eur J Pharm Biopharm* 2011;**77**(3):417-23, https://doi.org/10.1016/j.ejpb.2010.11.010.
32. Mahaling B, Verma M, Mishra G, Chaudhuri S, Dutta D, Sivakumar S. Fate of GdF3 nanoparticles-loaded PEGylated carbon capsules inside mice model: a step toward clinical application. *Nanotoxicology* 2020;**14**(5):577-94, https://doi.org/10.1080/17435390.2019.1708494.
33. Kaul G, Amiji M. Biodistribution and targeting potential of poly(ethylene glycol)-modified gelatin nanoparticles in subcutaneous murine tumor model. *J Drug Target* 2004;**12**(9–10):585-91, https://doi.org/10.1080/10611860400013451.
34. He Q, Zhang Z, Gao F, Li Y, Shi J. In vivo biodistribution and urinary excretion of mesoporous silica nanoparticles: effects of particle size and PEGylation. *Small* 2011;**7**(2):271-80, https://doi.org/10.1002/smll.201001459.
35. Takeuchi I, Onaka H, Makino K. Biodistribution of colloidal gold nanoparticles after intravenous injection: effects of PEGylation at the same particle size. *Biomed Mater Eng* 2018;**29**(2):205-15, https://doi.org/10.3233/BME-171723.
36. Lankveld DPK, Rayavarapu RG, Krystek P, et al. Blood clearance and tissue distribution of PEGylated and non-PEGylated gold nanorods after intravenous administration in rats. *Nanomedicine* 2011;**6**(2):339-49, https://doi.org/10.2217/nnm.10.122.
37. Li R, Eun JS, Lee MK. Pharmacokinetics and biodistribution of paclitaxel loaded in pegylated solid lipid nanoparticles after intravenous administration. *Arch Pharm Res* 2011;**34**(2):331-7, https://doi.org/10.1007/s12272-011-0220-2.
38. Yadav KS, Jacob S, Sachdeva G, Chuttani K, Mishra AK, Sawant KK. Long circulating PEGylated PLGA nanoparticles of cytarabine for targeting leukemia. *J Microencapsul* 2011;**28**(8):729-42, https://doi.org/10.3109/02652048.2011.615949.
39. Li Q, Wang Z, Chen Y, Zhang G. Elemental bio-imaging of PEGylated NaYF4:Yb/Tm/Gd upconversion nanoparticles in mice by laser ablation inductively coupled plasma mass spectrometry to study toxic side effects on the spleen, liver and kidneys. *Metallomics* 2017;**9**(8):1150-6, https://doi.org/10.1039/c7mt00132k.

40. Crawford LA, Watkins HC, Wayne E, Putnam D. Altered biodistribution and tissue retention of nanoparticles targeted with P-glycoprotein substrates. *Regen Eng Transl Med* 2019;**5**(3):308-18, https://doi.org/10.1007/s40883-019-00111-8.
41. Higuchi Y, Niidome T, Miyamoto Y, et al. Accumulation of gold nanorods in the failing heart of transgenic mice with the cardiac-specific expression of TNF-α. *Heart Vessels* 2019;**34**(3):538-44, https://doi.org/10.1007/s00380-018-1241-2.
42. Dong Z, Guo J, Xing X, Zhang X, Du Y, Lu Q. RGD modified and PEGylated lipid nanoparticles loaded with puerarin: formulation, characterization and protective effects on acute myocardial ischemia model. *Biomed Pharmacother* 2017;**89**:297-304, https://doi.org/10.1016/j.biopha.2017.02.029.
43. Shao M, Yang W, Han G. Protective effects on myocardial infarction model: delivery of schisandrin B using matrix metalloproteinase-sensitive peptide-modified, PEGylated lipid nanoparticles. *Int J Nanomedicine* 2017;**12**:7121-30, https://doi.org/10.2147/IJN.S141549.
44. Zhang S, Wang J, Pan J. Baicalin-loaded PEGylated lipid nanoparticles: characterization, pharmacokinetics, and protective effects on acute myocardial ischemia in rats. *Drug Deliv* 2016;**23**(9):3696-703, https://doi.org/10.1080/10717544.2016.1223218.
45. Daems N, Verlinden B, Van Hoecke K, et al. In vivo pharmacokinetics, biodistribution and toxicity of antibody-conjugated gold nanoparticles in healthy mice. *J Biomed Nanotechnol* 2020;**16**(6):985-96, https://doi.org/10.1166/jbn.2020.2928.
46. Zhang L, Tian XY, Chan CKW, et al. Promoting the delivery of nanoparticles to atherosclerotic plaques by DNA coating. *ACS Appl Mater Interfaces* 2019;**11**(15):13888-904, https://doi.org/10.1021/acsami.8b17928.
47. Rangaswami J, Bhalla V, JEA Blair, et al. *Cardiorenal Syndrome: Classification, Pathophysiology, Diagnosis, and Treatment Strategies: A Scientific Statement From the American Heart Association*, 139; 2019, https://doi.org/10.1161/CIR.0000000000000664.
48. Ronco C, McCullough P, Anker SD, et al. Cardio-renal syndromes: report from the consensus conference of the acute dialysis quality initiative. *Eur Heart J* 2010;**31**(6):703-11, https://doi.org/10.1093/eurheartj/ehp507.
49. Angelini A, Castellani C, Virzì GM, et al. The role of congestion in cardiorenal syndrome type 2: new pathophysiological insights into an experimental model of heart failure. *CardioRenal Med* 2015;**6**(1):61-72, https://doi.org/10.1159/000440775.
50. Liu Y, Yin L. α-Amino acid N-carboxyanhydride (NCA)-derived synthetic polypeptides for nucleic acids delivery. *Adv Drug Deliv Rev* 2021;**171**:139-63, https://doi.org/10.1016/j.addr.2020.12.007.
51. Wang LL, Liu Y, Chung JJ, et al. Local and sustained miRNA delivery from an injectable hydroel promotes cardiomyocyte proliferation and functional regeneratin after ischemic injury. *Nat Biomed Eng* 2018;**1**:983-92, https://doi.org/10.1038/s41551-017-0157-y.
52. Wang Y, Hou M, Duan S, et al. Macrophage-targeting gene silencing orchestrates myocardial microenvironment remodeling toward the anti-inflammatory treatment of ischemia-reperfusion (IR) injury. *Bioact Mater* 2021;**2022**(17):320-33, https://doi.org/10.1016/j.bioactmat.2022.01.026.
53. Yin B, Chan CKW, Liu S, et al. Intrapulmonary cellular-level distribution of inhaled nanoparticles with defined functional groups and its correlations with protein Corona and inflammatory response. *ACS Nano* 2019;**13**(12):14048-69, https://doi.org/10.1021/acsnano.9b06424.
54. Kang JY, Kim H, Mun D, Yun N, Joung B. Co-delivery of curcumin and miRNA-144-3p using heart-targeted extracellular vesicles enhances the therapeutic efficacy for myocardial infarction. *J Control Release* August 2020;**2021**(331):62-73, https://doi.org/10.1016/j.jconrel.2021.01.018.
55. Yu H, Li Y, Zhang R, et al. Inhibition of cardiomyocyte apoptosis post-acute myocardial infarction through the efficient delivery of microRNA-24 by silica nanoparticles. *Nanoscale Adv* 2021;**3**(22):6379-85, https://doi.org/10.1039/d1na00568e.
56. Gomez K, Mcvey JH. *Haemostasis and Thrombosis*. Hammersmith Hospital Campus, Du Cane Road, London W12 0NN. Sci York: MRC Clinical Sciences Centre, Imperial College London; 2006. p. 1349-59. Published online.
57. Ruiz-esparza GU, Segura-ibarra V, Cordero-reyes AM, et al. A specifically designed nanoconstruct associates, internalizes, traffics in cardiovascular cells, and accumulates in failing myocardium: a new strategy for heart failure diagnostics and therapeutics. *Eur J Heart Fail* 2016;**18**(2):169-78, https://doi.org/10.1002/ejhf.463.A.